

# Ionized gaseous nebulae chemical abundance determination using the direct method

Enrique Pérez-Montero

Instituto de Astrofísica de Andalucía - CSIC. Apdo. 3004, 18080, Granada, Spain

In this tutorial it is explained the procedure to analyze an optical emission-line spectrum produced by a nebula ionized by massive star formation. Particularly, it is described the methodology used to derive physical properties, such as electron density and temperature, and the ionic abundances of the most representative elements whose emission lines are present in the optical spectrum. The tutorial is focused on the direct method, based on the measurement of the electron temperature to derive the abundances, given that the ionization and thermal equilibrium of the ionized gas is dominated by the metallicity. The ionization correction factors used to obtain total abundances from the abundances of some of their ions are also given. Finally, some strong-line methods to derive abundances are described. These are used when no estimation of the temperature can be derived, but that can be consistent with the direct method if they are empirically calibrated.

## 1. Introduction

The determination of chemical abundances is one of the goals of the analysis of the emission-line spectra produced by the ionization of a gas cloud by massive stars. By deriving the relative amount of metals in the gas it is possible to give valuable constraints to the past chemical enrichment and star formation history as these elements can only be produced by nucleosynthesis in the star-cores before their ejection into the interstellar medium. The relations between metallicity and other observational properties in the studied objects have important implications in different scales and environments. For instance, the integrated metallicity of star-forming galaxies correlates with stellar mass or star formation rate. Its distribution across galactic radii in spiral galaxies depends on the evolution of the disks, the search for the fraction of primordial helium can constrain other important cosmological parameters (e.g. Peimbert & Luridiana (2002), Peimbert et al. (2007)), and in planetary nebulae or envelopes or massive stars the study of chemical abundances allows us to analyze stellar evolution.

The processes of massive star formation irradiate light at all wavelengths, including the energetic UV and X-ray able to pull up the electrons in the atoms of the surrounding gas clouds. As a consequence the atoms of the gas are excited and ionized, forming a plasma with free electrons, protons and ions. When the protons and ions recapture the free electrons of the resulting plasma, they re-emit the radiation under the form of bright lines as the electrons fall from level to level towards their ground state orbiting around nuclei. These electron recombinations are in equilibrium with the constant process of photoionization. Since the typical electron temperature of the nebular plasma is of the same order than the photons at the optical wavelength the lines emitted by the gas are prominent and many times dominate the luminosity of the ionized gas and even of entire starburst galaxies. In Fig. 1 it can be seen a typical emission-line optical spectrum of a H II region and in Table 1 a list of the most prominent emission lines with their wavelengths can be found.

Among the different emission lines that can be found in an H II region spectrum, there are the recombination lines (RLs), weakly dependent on the nebular internal temperature.

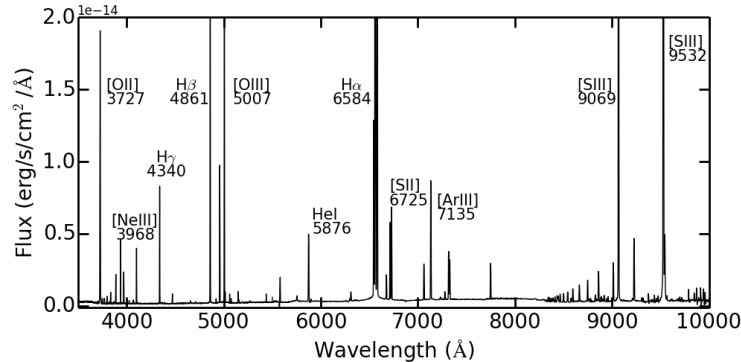


FIGURE 1. Optical spectrum of the Galactic H II region S-156 as taken with the ISIS spectrograph mounted on the William Herschel Telescope (WHT) (Fernández-Martín et al.(2017))

Most of the brightest lines emitted by the lightest elements (H, He) are of this type. In the case of metals (i.e. all elements heavier than He) RLs provide more precise abundance determinations (i.e. with a precision better than 5%) but they are very weak (i.e. around  $10^{-4}$  times fainter than H $\beta$  4861 Å) and thus difficult to measure in weak or distant objects. Instead, collisional excited lines (CELs) are much brighter and easier to be detected in optical spectra. These lines correspond to transitions forbidden owing to their very low quantum probabilities, but that dominate the cooling of the gas under the extremely low densities of the gas in these nebulae. The intensities of these CELs depend exponentially on the temperature. In principle, the temperature can be determined from appropriate line intensity ratios which however require the detection and measurement of intrinsically faint (or absent) auroral lines. This is in particular the case for regions with high metal content – for which the cooling produced by the metals is very efficient and the lines are no longer detected – and also for distant H II regions and regions with low surface brightness. In Table 1 it is also listed the nature of the emission lines usually observed in the optical spectrum, attending to RLs, nebular CELs and auroral CELs.

In those cases where no auroral lines are measured with confidence in the optical spectrum, other methods based on the strong nebular line intensities are used. However one must take into account that in many cases, calibrations are obtained from photoionization models for which the uncertainties are difficult to quantify and lead to absolute metallicity values not always compatible with the values obtained from the direct method. See for instance Kewley & Ellison(2008) to see differences between direct method metallicities and other obtained from strong-line methods based on models. In contrast, see Dors et al.(2011) or Pérez-Montero(2014) to see other sets of models that lead to chemical abundances not systematically higher than those derived from the direct method.

In any case, even when the electronic temperature can be determined with high precision, there are some problems limiting the confidence on the attained results following the direct method. Those problems include: (1) the effect of the internal ionization structure on multiple zone models (Pérez-Montero & Díaz(2003)); (2) temperature fluctuations across the nebula (Peimbert(2003)); (3) collisional and density effects on the ionic temperatures (Luridiana et al.(1999)); (4) neutral gas zones affecting the determination of ionization correction factors (ICFs)(Peimbert & Luridiana (2002)); (5) the ionization structure is not adequately described by present models (Pérez-Montero & Díaz(2003)); (6) possible photon escape affecting low ionization lines in the outer regions of the nebula

TABLE 1. List and properties of the most prominent optical emission lines, including wavelength, ion, nature (RL for recombination line, CEL ( $n$ ) for nebular collisional line and CEL ( $a$ ) for collisional auroral line) and extinction coefficient using the law by Cardelli et al.(1989).

$\lambda$ (Å)	Ion	Class	$f(\lambda)$	$\lambda$ (Å)	Ion	Class	$f(\lambda)$
3726.0	[O II]	CEL -( $n$ )	0.322	5875.6	HeI	RL	-0.203
3728.8	[O II]	CEL - ( $n$ )	0.322	6300.3	[OI]	CEL ( $n$ )	-0.263
3868.8	[Ne III]	CEL ( $n$ )	0.291	6312.1	[S III]	CEL ( $a$ )	-0.264
3967.5	[Ne III]	CEL ( $n$ )	0.266	6363.8	[OI]	CEL ( $n$ )	-0.272
3970.0	H7	RL	0.256	6548.1	[N II]	CEL ( $n$ )	-0.295
4068.7	[S II]	CEL ( $a$ )	0.239	6563.0	H $\alpha$	RL	-0.298
4076.4	[S II]	CEL ( $a$ )	0.237	6583.5	[N II]	CEL ( $n$ )	-0.304
4102.0	H $\delta$	RL	0.229	6678.0	HeI	RL	-0.313
4340.0	H $\delta$	RL	0.157	6716.4	[S II]	CEL ( $n$ )	-0.318
4363.2	[O III]	CEL ( $a$ )	-0.149	6730.8	[S II]	CEL ( $n$ )	0.320
4471.5	HeI	RL	0.10.115	7065.0	HeI	RL	-0.364
4668.1	[Fe III]	CEL ( $n$ )	0.058	7135.8	[Ar III]	CEL ( $n$ )	-0.378
4686.0	HeII	RL	0.050	7319.5	[O II]	CEL ( $a$ )	-0.398
4711.3	[Ar III]	CEL ( $n$ )	0.042	7330.2	[O II]	CEL ( $a$ )	-0.400
4713.1	HeI	RL	0.042	9017.4	H I P10	RL	-0.590
4740.1	[Ar IV]	CEL ( $n$ )	0.038	9068.6	[S III]	CEL ( $n$ )	-0.594
4861.0	H $\beta$	RL	0.000	9231.5	H I - P9	RL	-0.605
4958.9	[O III]	CEL ( $n$ )	-0.026	9530.6	[S III]	CEL ( $n$ )	-0.625
5006.9	[O III]	CEL ( $n$ )	-0.038	9548.6	H I P8	RL	-0.626
5754.6	[N II]	CEL ( $a$ )	-0.185				

(Castellanos et al.(2002)). The first three effects can introduce uncertainties regarding the derived O abundance of some 0.2, 0.3 and 0.4 dex respectively, depending on the degree of excitation. The uncertainties associated to the rest of the enumerated problems have not yet been quantified.

In this tutorial some very basic instructions to derive physical properties and ionic chemical abundances following the direct method are given. The basic assumptions behind these calculations are mainly two: i) the gas is ionized by hot massive stars whose spectral every distribution can be modeled by a black-body and ii) all the emission from the ionized gas, including its complete ionization structure (i.e. from the innermost layer irradiated by the star up to the photodissociation region, where the gas is neutral or the outer edge is reached) is well traced by the observed spectrum.

For this work, all  $n_e$ ,  $T_e$  and ionic abundances were re-calculated using expressions derived using non-linear fittings to the results obtained from the emission-line analysis software PYNEB v0.9.3 (Luridiana et al.(2012)) as described below and with the most updated sets of atomic coefficients. The expressions were obtained using arbitrary sets of input emission-line intensities covering the most common conditions and some of them can be also found in Pérez-Montero(2014) or Dors et al.(2016). These formulae are provided to ease the reproducibility of the calculations, the error analysis and their applicability for large data samples using different software.

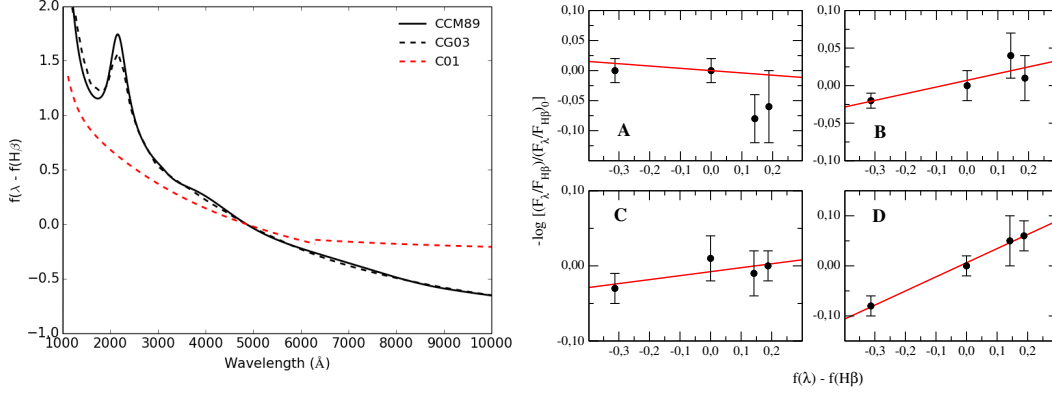


FIGURE 2. At left, different extinction laws including Cardelli et al.(1989) (solid black line), Gordon et al.(2003) for the LMC (black dashed line), and Calzetti et al.(2000) (red dashed line). At right, linear fittings to the theoretical-to-observed H I emission lines to obtain the reddening constants in four knots of star formation in the galaxy IIZw71 (Pérez-Montero et al.(2009)).

## 2. Emission-line measurement and extinction

Once an optical spectrum is conveniently reduced, calibrated and extracted, the analysis of the emission lines must lead to the measurement of their integrated fluxes in units of  $\text{erg}\cdot\text{s}^{-1}\cdot\text{cm}^{-2}$ , reddening corrected and usually relative to an H I line, usually H $\beta$ .

The main source of uncertainty associated to the derived physical properties are related with the error of the fluxes of the lines. The measure of these fluxes can be either done manually (e.g. using the IRAF TASK SPLOT) OR USING OTHER AUTOMATIC ROUTINES THAT FIT A GAUSSIAN FUNCTION TO THE LINE PROFILE. These programs can integer the intensity of each line over a local continuum. The errors of the fluxes measured in this way can be calculated with the expression from Gonzalez-Delgado et al.(1994):

$$\sigma_l = \sigma_c \cdot \sqrt{N + \frac{EW}{\Delta}} \quad (2.1)$$

where  $\sigma_l$  is the error of flux of the line,  $\sigma_c$  represents the standard deviation in a box near of the measured emission line and represents the error in the position of the continuum,  $N$  is the number of pixels in the measure of the flux of the line,  $EW$  is the equivalent width of the line and  $\Delta$  is the dispersion of the wavelength in angstroms per pixel. If a Gaussian function fitting is used to integer the fluxes, this expression should be added quadratically to the uncertainty of the fitting, as well as with other known sources of uncertainty, as flux calibration error. The use of any automatic routine to measure emission-line fluxes should consider all these sources of uncertainty in the final error balance.

A previous treatment of the underlying stellar continuum can help to reduce the uncertainty, above all if the recombination H and He lines are clearly affected by stellar absorption. Hence, an appropriate subtraction of this emission before the measurement of the emission lines is convenient using fitting of synthetic stellar populations (e.g. STARLIGHT, Cid Fernandes et al.(2005)).

Another important source of uncertainty that can affect the resulting abundances from the direct method is owing to extinction correction. The gas is mixed with dust grains that absorb and scatter part of the optical emission to re-emit it in the infrared affecting

the relative emission line fluxes. Hence, each one of the intensities measured in this way must be reddening corrected. The physical law that describes the extinction of a certain emission line at a certain  $\lambda$  in units of Å is:

$$F_0(\lambda) = 10^{-\tau_\lambda} \cdot F_{obs}(\lambda) = 10^{(1+c(H\beta)) \cdot f(\lambda)} \cdot F_{obs}(\lambda) \quad (2.2)$$

where  $F_0$  is the corrected emission line flux,  $F_{j_{obs}}$  is the measured flux and  $\tau_\lambda$  is the optical depth at a certain wavelength,  $c(H\beta)$  is the reddening constant, what defines the amount of extinction at the wavelength of H $\beta$ . Finally,  $f(\lambda)$  is the extinction law, what defines the behavior of the extinction as a function of wavelength. In left panel of Fig. 2 can be seen different extinction laws including Cardelli et al.(1989) for the Milky Way, Gordon et al.(2003) for the Large Magellanic Cloud, or Calzetti et al.(2000) for starburst galaxies. These laws present differences above all in the ultraviolet part of the spectrum. In Table 1 can also seen the values of  $f(\lambda) - f(H\beta)$  according to Cardelli et al.(1989), assuming a value of  $R_V = 3.1$  (i.e.  $R_V$  is defined as the ratio  $A_V/(A_V - A_B)$  and  $A_V$  and  $A_B$  are the extinctions in mag for bands V and B, respectively).

The reddening constant  $c(H\beta)$  can be calculated from the decrement of Balmer of the stronger recombination lines of hydrogen. We can write this expression in order to calculate the reddening correction as a function of the H $\beta$  flux as:

$$\frac{I_0(\lambda)}{I_0(H\beta)} = \frac{I_{obs}(\lambda)}{I_{obs}(H\beta)} \cdot 10^{c(H\beta) \cdot [f(\lambda) - f(H\beta)]} \quad (2.3)$$

Then,  $c(H\beta)$  can be derived comparing the observed flux ratios between the most prominent hydrogen recombination lines and the theoretical expected values, which depend on density and temperature. In Table 2 are listed the expected values between the flux of H $\beta$  and other H $\alpha$  lines as predicted using data from Storey & Hummer(1995) in the case B (i.e. photons are absorbed as soon as they are emitted). Using this same data set López-Sánchez et al.(2015) provide a polynomial fitting of the theoretical Balmer ratios as a function of temperature in units of K for a fixed density of  $100 \text{ cm}^{-3}$ . the resulting fittings are the following:

$$\frac{I(H\alpha)}{I(H\beta)} = 10.35 - 3.254 \cdot \log T_e + 0.3457 \cdot (\log T_e)^2 \quad (2.4)$$

$$\frac{I(H\gamma)}{I(H\beta)} = 0.0254 + 0.1922 \cdot \log T_e - 0.0204 \cdot (\log T_e)^2 \quad (2.5)$$

$$\frac{I(H\delta)}{I(H\beta)} = -0.07132 + 0.1436 \cdot \log T_e - 0.0153 \cdot (\log T_e)^2 \quad (2.6)$$

although other ratios for different atomic data can also be found in Osterbrock & Ferland.

Then the reddening constant can be derived using a linear fitting, as in Fig. 2 or for doublets of lines as of H $\alpha$  and H $\beta$  when the other recombination H $\alpha$  lines are very faint. Since the calculation of reddening depends on temperature and density, if the derived temperature deviates much from the adopted value, it is better to make an iterative analysis to check the consistency of the calculated extinction. When the resulting

TABLE 2. Theoretical H I flux ratios as a function of density and temperature using Storey &amp; Hummer(1995) data under case B approximation.

Ratio	$n_e = 100 \text{ cm}^{-3}$				$n_e = 1000 \text{ cm}^{-3}$			
	7 500 K	10,000 K	15,000 K	20,000 K	7,500 K	10,000 K	15,000 K	20,000 K
H $\alpha$ /H $\beta$	2.93	2.86	2.79	2.75	2.92	2.86	2.78	2.74
H $\gamma$ /H $\beta$	0.464	0.468	0.473	0.475	0.465	0.469	0.473	0.475
H $\delta$ /H $\beta$	0.256	0.259	0.262	0.264	0.256	0.259	0.263	0.264
P10/H $\beta$	0.0189	0.0184	0.0177	0.0172	0.0189	0.0184	0.0177	0.0172
P8/H $\beta$	0.0376	0.0366	0.0350	0.0339	0.0376	0.0366	0.0350	0.0339

reddening constant is negative, it is usually assumed that no dust attenuation is produced and no reddening correction is applied to the relative emission lines.

The uncertainty associated with the reddening correction must be taken into the account in the errors of the emission lines and conveniently propagated into all the physical magnitudes we calculate. Nevertheless, one way to minimize this uncertainty is to correct a given emission line relative to its closest H I line in wavelength and then using the theoretical ratio to H $\beta$ .

In the case of integrated spectra from galaxies or extragalactic H II regions, one has to take care that the mechanism of ionization is not different than massive stars (e.g. active galactic nucleus, shocks, post-AGB stars) with a spectral energy distribution that can make the ionization equilibrium to be different. In these cases the derivation of the extinction, the physical properties or the chemical abundances using this prescription is not possible. Normally AGNs can be identified by means of X-ray emission or the use of adequate diagnostic diagrams (e.g. BPT Baldwin et al.(1981), see also Kewley et al.(2006)). See also Sánchez et al.(2015) for a description of other methods of selection of star-forming regions.

### 3. Electron temperature and density

The thermal and density structure of H II regions can be obtained by means of the measurement of the fluxes of their emission-lines. The direct method relies completely on the measurement of at least one auroral emission line and the radial thermal structure can be derived using as many measured temperatures as possible or assuming the temperature of the different zones from the measured values. In Fig. 3 we see two examples of thermal structure, one owing to photoionization models and the other to the measurement of different line diagnostics in a  $t - n$  diagram. The relation between these temperatures is not many times simple and depends on factors such as density profile, dust-to-gas ratio, geometry of the gas (matter or density-bounded), so the most accurate method is to get as many temperature diagnostics as possible to derive consistently the chemical abundances of each ion.

One simple sketch of the thermal inner structure is the one proposed by Garnett(1992) assuming three different zones: i) the *high-excitation* zone, which is the innermost, and corresponds to  $t([\text{O III}])$  ( $t_h$ ), ii) the *low-excitation* zone, which is the outermost, and corresponds to electron temperatures such as  $t([\text{O II}])$ ,  $t([\text{S II}])$  or  $t([\text{N II}])$  ( $t_l$ ). Finally, iii) the *intermediate excitation* zone appears between these two and it is mainly represented by  $t([\text{S III}])$  ( $t_m$ ).

Another limitation to calculate the physical properties is the dependence of the de-

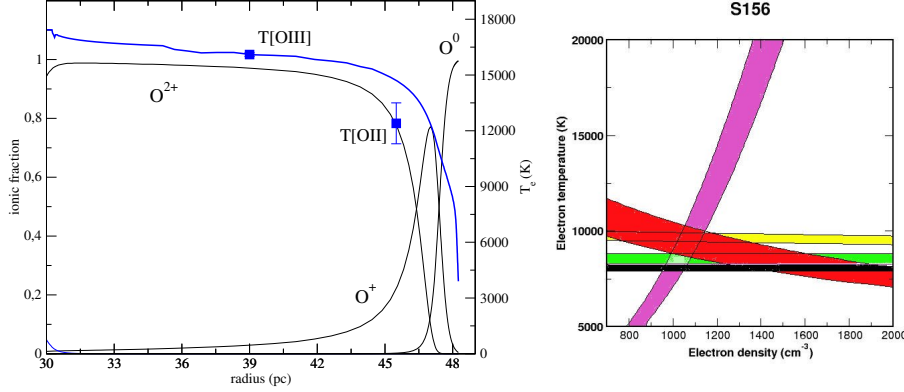


FIGURE 3. Two examples of the thermal and density structure of the gas in H II regions: Left, radial profile of oxygen abundances and temperature in the brightest knot of the blue compact dwarf galaxy Mrk 209 as derived from models (Pérez-Montero & Díaz(2007)). Right: Diagnostic empirical  $n - T$  diagram for the H II region Sh-156 Fernández-Martín et al.(2017). Blue band corresponds to  $n([S II])$ , black to  $t([O III])$ , yellow to  $t([N II])$ , red to  $t([S II])$ , and green to  $t([S III])$ .

rived electron temperatures on density and vice versa. This is usually overcome using an iterative method if the assumed initial conditions deviate much from the results, or using diagnostic diagrams as the one shown in right panel of Fig. 3.

In this section, it is described the expressions to derive them from the strongest collisional lines usually observed in the optical spectrum.

### 3.1. Oxygen

The  $T_e$  of [O III] can be calculated from the emission-line ratio:

$$R_{O3} = \frac{I(4959) + I(5007)}{I(4363)} \quad (3.1)$$

given that, according to Osterbrock & Ferland, temperature can be obtained from the ratio of collisional transitions that have a similar energy but occupy different levels. In this calculation it is not required to measure the two strong [O III] lines as there is a theoretical ratio between them ( $I(5007) = 3 \cdot I(4959)$ ). The fitting between the ratio and the electronic temperature was obtained using the program PYNEB assuming a five level atom and the following non-linear fitting for  $n_e = 100 \text{ cm}^{-3}$ :

$$t([O III]) = 0.7840 - 0.0001357 \cdot R_{O3} + \frac{48.44}{R_{O3}} \quad (3.2)$$

in units of  $10^4 \text{ K}$ , valid in the range  $t = 0.7 - 2.5$  and using collisional strengths from Aggarwal & Keenan(1999). This fitting gives precisions better than 1% for  $1.0 < t([O III]) < 2.5$ , and better than 3% for  $0.7 < t([O III]) < 1.0$ . It was calculated for a density of  $100 \text{ cm}^{-3}$ , but considering a density of  $1000 \text{ cm}^{-3}$  reduces the temperature only in a 0.1%. This relation with the resulting fitting can be seen in left panel of Fig. 4.

For [O II] the quotient for the electron temperature is calculated from

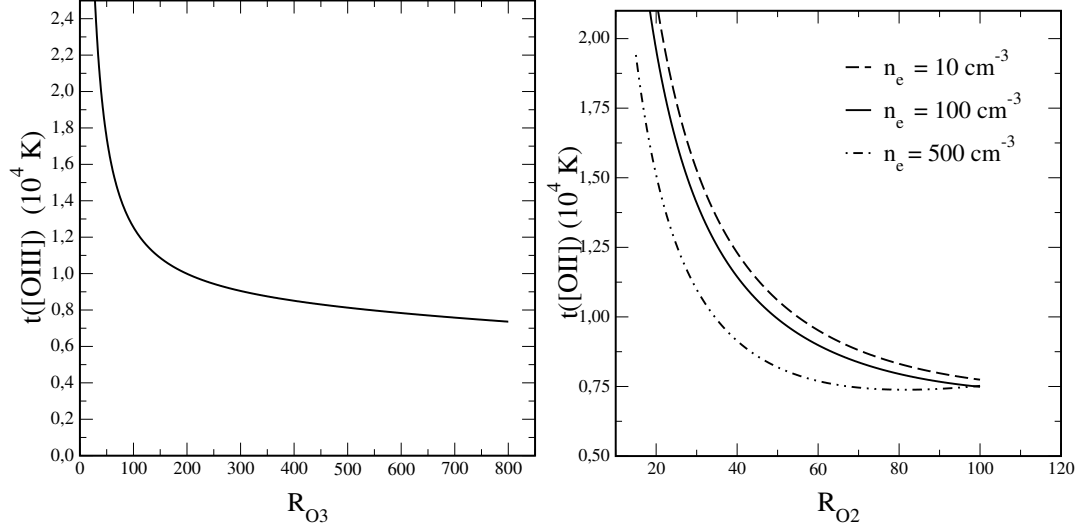


FIGURE 4. Relations between the corresponding nebular-to-auroral lines and the electron temperature for [O III] (left) and [O II] (right). In this last case, as a function of the electron density.

$$R_{O2} = \frac{I(3726) + I(3729)}{I(7319\text{\AA}) + I(7330\text{\AA})} \quad (3.3)$$

One has to be careful in this case, because the [O II] auroral lines might be contaminated by recombination emission. Such emission however, can be quantified and corrected, according to Liu et al.(2001), as such contribution can be fitted (for  $0.5 \leq t \leq 1.0$ ) by the function:

$$\frac{I_R(7319 + 7330)}{I(H\beta)} = 9.36 \cdot t^{0.44} \cdot \frac{O^{2+}}{H^+} \quad (3.4)$$

Moreover, the ratio of the [O II] lines is strongly dependent on the electron density. Ideally, one should know the [O II] density from the ratio  $I(3726\text{\AA})/I(3729\text{\AA})$  but very frequently we lack resolution to separate the doublet in which case one has to resort to the [S III] density, also representing the low excitation zone. The fitting obtained is:

$$t([O II]) = a_0(n) + a_1(n) \cdot R_{O2} + \frac{a_2(n)}{R_{O2}} \quad (3.5)$$

that also gives  $t$  in units of  $10^4$  K and where the coefficients are respectively:

$$a_0(n) = 0.2526 - 0.000357 \cdot n - \frac{0.43}{n}$$

$$a_1(n) = 0.00136 + 5.42 \cdot 10^{-6} \cdot n + \frac{0.00481}{n}$$



$$a_2(n) = 35.624 - 0.0172 \cdot n + \frac{25.12}{n} \quad (3.6)$$

being  $n$  the electron density in units of  $\text{cm}^{-3}$  and using the collisional coefficients from Pradhan et al.(2006) and Tayal(2007). The fittings were made in the range  $t = 0.8 - 2.5$  in units of  $10^4$  K with an uncertainty better than 2%. The resulting fittings for different electron densities can be seen in right panel of Fig. 4.

Often the auroral [O II] lines are not observed with good S/N or they are outside our observed spectral range. In that case it is practical to use some relation based on photoionization models in order to infer  $t[\text{O II}]$  from  $t[\text{O III}]$ . For instance, the relation

$$t([\text{O II}]) = \frac{2}{t([\text{O III}])^{-1} + 0.8} \quad (3.7)$$

based on Stasińska(1990) models is frequently accepted. However, such expression neglects the dependence of  $t[\text{O II}]$  on the density, consistent with the dispersion for the objects for which both temperatures have been derived from observations as can be seen in left upper panel of Fig. 5. In the same panel are shown fittings to grids of models, presented in Pérez-Montero & Díaz(2003), with different electron densities. The density-dependent calibration obtained in this case and given in Hägele et al.(2006) is:

$$t([\text{O II}]) = \frac{1.2 + 0.002 \cdot n + \frac{4.2}{n}}{t([\text{O III}])^{-1} + 0.08 + 0.003 \cdot n + \frac{2.5}{n}} \quad (3.8)$$

### 3.2. Sulfur

The [S II] line ratio is commonly used to determine electron density for the low excitation zone. It is generally assumed that the nebula has constant density, although there is growing evidence for the existence of a density profile instead. Fortunately, the high excitation species have diagnostic ratios that are almost no density sensitive.

Electron densities are necessary for the derivation of chemical abundances of ions of the type  $\text{np}^2$ , such as  $\text{O}^+$ . These densities were derived using the following emission-line ratio:

$$R_{S2} = \frac{I(6716)}{I(6731)} \quad (3.9)$$

The following expression is proposed to derive the electron density:

$$n_e([\text{S II}]) = 10^3 \cdot \frac{R_{S2} \cdot a_0(t) + a_1(t)}{R_{S2} \cdot b_0(t) + b_1(t)} \quad (3.10)$$

with  $n_e$  in units of  $\text{cm}^{-3}$  and  $t$  in units of  $10^4$  K. Using the appropriate fittings and PYNEB with collision strengths from Tayal & Zatsarinny(2010) gives these polynomial fittings to the coefficients

$$a_0(t) = 16.054 - 7.79/t - 11.32 \cdot t$$

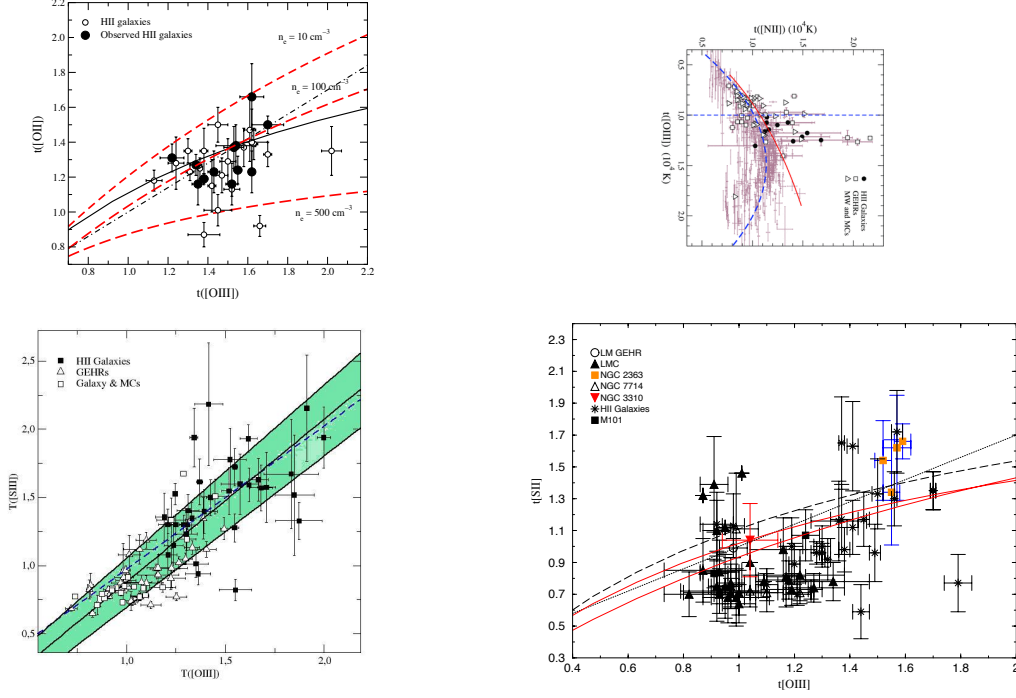


FIGURE 5. Empirical and model-based relations between different line temperatures: In the upper left panel, relation between  $t([O\text{ III}])$  and  $t([O\text{ II}])$  (Pérez-Montero & Díaz(2003)), in the upper right, relation between  $t([O\text{ III}])$  and  $t([N\text{ II}])$  (Pérez-Montero & Contini(2009)). In the upper right panel, relation between  $t([O\text{ III}])$  and  $t([S\text{ III}])$  (Hägele et al.(2006)) and in the lower right panel, relation between  $t([O\text{ III}])$  and  $t([S\text{ II}])$  (Pérez-Montero(2003)).

$$\begin{aligned}
 a_1(t) &= -22.66 + 11.08/t + 16.02 \cdot t \\
 b_0(t) &= -21.61 + 11.89/t + 14.59 \cdot t \\
 b_1(t) &= 9.17 - 5.09/t - 6.18 \cdot t
 \end{aligned} \tag{3.11}$$

This expression fits the density calculated by PYNEB better than a 1% for temperatures in the range  $0.6 < t_e < 2.2$  and densities in the range  $10 < n_e < 1000$ .

here  $t$  is generally  $t([O\text{ III}])$ , although an iterative process could be used to calculate it with  $t([S\text{ III}])$  given that this temperature, like  $t([O\text{ II}])$ , a type  $np^3$  ion, is density dependent. The ratio used in this case is:

$$R'_{S2} = \frac{I(6717) + I(6731)}{I(4068) + I(4076)} \tag{3.12}$$

For the  $[S\text{ II}]$  auroral lines it is enough to measure one of them, as they are related by a fixed theoretical ratio,  $I(4068\text{\AA}) \approx 3 \cdot I(4076\text{\AA})$ . We can calculate in this way the  $[S\text{ II}]$  temperature.

$$t([\text{S II}]) = a_0(n) + a_1(n) \cdot R'_{S2} + \frac{a_2(n)}{R'_{S2}} + \frac{a_3(n)}{R'^2_{S2}} \quad (3.13)$$

where

$$\begin{aligned} a_0(n) &= 0.99 + \frac{34.79}{n} + \frac{321.82}{n^2} \\ a_1(n) &= -0.0087 + \frac{0.628}{n} + \frac{5.744}{n^2} \\ a_2(n) &= -7.123 + \frac{926.5}{n} - \frac{94.78}{n^2} \\ a_3(n) &= 102.82 + \frac{768.852}{n} - \frac{5113}{n^2} \end{aligned} \quad (3.14)$$

also fitted with the coefficients by Tayal & Zatsarinny(2010) in the range  $t = 0.8$  to  $2.5$  in units of  $10^4$  K and  $n_e$  up to  $500 \text{ cm}^{-3}$  with a precision better than 2%.

When the  $[\text{S II}]$  auroral lines are not available, it is usually assumed that  $t([\text{S II}]) \approx t([\text{O II}])$ . There is evidence however, suggesting a somewhat lower value. From the models used in Pérez-Montero(2003), it is obtained a lineal fitting:

$$t([\text{S II}]) = 0.71 \cdot t([\text{O II}]) + 0.12 \quad (3.15)$$

for a  $100 \text{ cm}^{-3}$  number density. For lower densities, this expression seems to be valid. In any case, for the few objects for which we have a simultaneous measurement of both temperatures, the dispersion is quite large as can be seen in lower left panel of Fig. 5 for H II galaxies.

Direct measurements of the  $[\text{S III}]$  temperature become possible with the availability of the collisional lines in the near IR.

$$R_{S3} = \frac{I(9069) + I(9532)}{I(6312)} \quad (3.16)$$

This expression can be simplified in case of lacking one of the near IR lines, knowing that  $I(9532\text{\AA}) \approx 2.44 \cdot I(9069\text{\AA})$ . With this ratio it is possible the corresponding temperature with the following fitting in the range  $t = 0.6 - 2.5$  using the collision strengths from Hudson et al.(2012)]Hudson, Ramsbottom, & Scott

$$t([\text{S III}]) = 0.5147 + 0.0003187 \cdot R_{S3} + \frac{23.64041}{R_{S3}} \quad (3.17)$$

with a precision better than 1% in the range  $0.6 < t([\text{S III}]) < 1.5$ , and better than 3% up to values  $t([\text{S III}]) = 2.5$ . These values enhance in less than a 3% when the considered density goes from 100 to  $1000 \text{ cm}^{-3}$ .

As discussed in Garnett(1992),  $t[\text{S III}]$  is in between the temperatures of  $[\text{O III}]$  and of  $[\text{O II}]$  and allows us to calculate the  $\text{S}^{2+}$  abundance from just the 6312 Å line in high-metallicity objects. In case that the  $[[\text{S III}]]$  cannot be measured, it is possible to derive  $t([[\text{S III}]])$  from  $t([\text{O III}])$ . and viceversa The empirical fitting given by Hägele et al.(2006) is:

$$t([\text{S III}]) = (1.19 \pm 0.08) \cdot t([\text{O III}]) - (0.32 \pm 0.10) \quad (3.18)$$

which can be seen in left lower panel of Fig. 5.

### 3.3. Nitrogen

The  $T_e$  of  $[\text{N II}]$  can be calculated using the ratio:

$$R_{N2} = \frac{I(6548) + I(6583)}{I(5755)} \quad (3.19)$$

that, with the corresponding fitting leads to the expression:

$$t([\text{N II}]) = 0.6153 - 0.0001529 \cdot R_{N2} + \frac{35.3641}{R_{N2}} \quad (3.20)$$

also in units of  $10^4$  K, in the range  $t = 0.6 - 2.2$  using collision strengths from Tayal(2011). This fit gives a precision better than 1% in the range  $0.7 < t([[\text{N II}]]) < 2.2$  and better than 3% in the range  $0.6 < t([[\text{N II}]]) < 0.7$ . It was calculated for a density of  $100 \text{ cm}^{-3}$ , but for a density of  $1000 \text{ cm}^{-3}$ , the temperature is reduced in less than a 1%.

The nebular lines of  $[\text{N II}]$  are very close to  $\text{H}\alpha$  so they appear sometimes blended to this line and therefore it is not possible to measure both of them. In this case it is often assumed the following theoretical relation between them,  $I(6583) \approx 2.9 \cdot I(6548)$ . Besides, the auroral line of  $[\text{N II}]$  is affected by recombination emission, that can be corrected using the next expression proposed by Liu et al.(2001):

$$\frac{I_R(5755)}{I(\text{H}\beta)} = 3.19 \cdot t^{0.30} \cdot \frac{N^{2+}}{H^+} \quad (3.21)$$

in the range between 5 000 and 20 000 K.

Unfortunately, the auroral line has very low signal-to-noise ratio, so it is usually considered the approximation  $t([\text{N II}]) \approx t([\text{O II}])$  as valid. This relation is confirmed by photoionization models but is quite sensitive to density and the inner ionization structure of the nebula, and it is possible to reach values closer to  $t([\text{S III}])$  in some cases, so in all case it can't be taken without any sort of uncertainty.

Other possibility is to calculate  $t([\text{N II}])$  directly from  $t([\text{O III}])$  using the expression derived using photoionization models by Pérez-Montero & Contini(2009), as can be seen in lower right panel of Fig. 5:

$$t([\text{N II}]) = \frac{1.85}{t([\text{O III}])^{-1} + 0.72} \quad (3.22)$$

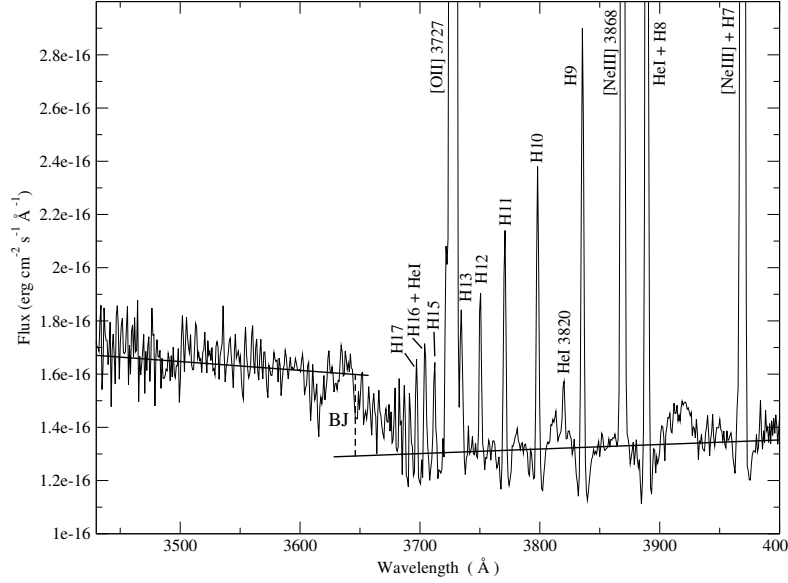


FIGURE 6. Measurement of the Balmer jump in the H II galaxy SDSS J003218.60+150014.2 in Hägele et al.(2006). The solid lines traces the continuum to both sides of the Balmer jump and the dashed line depicts the value of its measurement.

### 3.4. Balmer temperature

The Balmer temperature is an alternative to other temperatures calculated using collisionally excited lines. It depends on the value of the Balmer jump (BJ) in emission (i.e. the continuum nebular emission at a bluer wavelength than the Balmer series). In order to measure this value, it is necessary to fit the continuum in both sides of the discontinuity ( $\lambda_B = 3646 \text{ \AA}$ ). An example of the measurement of the BJ in an the optical spectrum of an H II galaxy can be seen in Fig. 6.

The contribution of the underlying stellar population affects, between other factors, to the emission of hydrogen lines near from the BJ. The increment in the number of lines at shorter wavelengths produces blends between them that trend to reduce the level of the continuum at a redder wavelength of the discontinuity so it is necessary to take into the account all this in the final uncertainty. Once measured the BJ, the Balmer temperature ( $T(\text{Bac})$ ) is measured from the quotient of the flux of the jump and the emission of the line H11 by means of the expression given in Liu et al.(2001):

$$T(\text{Bac}) = 368 \times (1 + 0.259y^+ + 3.409y^{++}) \left( \frac{BJ}{H11} \right)^{-3/2} K \quad (3.23)$$

where  $y^+$  and  $y^{++}$  are the ionic abundances of helium once and twice ionized, respectively, and BJ is in  $\text{ergs cm}^{-2} \text{ s}^{-1} \text{ \AA}^{-1}$ .

### 3.5. Other temperatures and densities

There are other collisional excited lines for other ions in the optical spectrum, but their corresponding temperatures or densities cannot be directly measured using the appropriate emission line ratios in the optical or their auroral lines are too weak to be detected. This is the case for [ArIV] for instance, for which we can derive the density in the inner nebula, or the temperatures of the rest of ions for which the corresponding auroral line are not available in the observed spectral range or there is not enough signal-to-noise ratio to detect their recombination lines. In this case, it is usually taken some assumptions about the gas structure and the position of each species is associated to another ion whose temperature is known. This is the case of the next ions, assuming the three-zone temperature sketch proposed by Garnett(1992):

$$t([\text{NeIII}]) \approx t([\text{FeIII}]) \approx t(\text{HeII}) \approx t([\text{ArIV}]) \approx t([\text{OIII}]) \approx t_h \quad (3.24)$$

$$t([\text{ArIII}]) \approx t([\text{SIII}]) \approx t_m \quad (3.25)$$

$$t([\text{SII}]) \leq t([\text{NII}]) \approx t([\text{OII}]) \approx t_l \quad (3.26)$$

## 4. Ionic and total chemical abundances

In what follows I will describe the expressions used to derive the chemical abundances of the ions whose emission lines can be measured in the optical spectrum. These formulae use the appropriate electron densities and temperatures obtained in the determination of the thermal structure of the gas. Most of the fittings follow equations with the same mathematical relations than those proposed by Pagel et al.(1992).

In addition, in order to derive total chemical abundances, the ionization correction factor for each species will be also described. ICFs are used to calculate total abundances from the observed ions of that element in the optical range, that usually do not fulfill all the ionic stages present in the gas.

$$\frac{N(X)}{N(H)} = ICF(X_{obs}) \cdot \frac{N(X_{obs})}{N(H^+)} \quad (4.1)$$

### 4.1. Helium

Helium lines, as equal as hydrogen ones in the visible spectrum, have a recombination nature and they are generally strong and numerous, although many of them are usually blended with other lines. Besides they are affected by absorption of underlying stellar population, by fluorescence or by collisional contribution.

The total He abundance can be calculated in the optical spectrum using lines of HeI and HeII. Following the same equations as described in Olive & Skillman(2004), Once

subtracted the stellar absorption and reddening correction has been carried out, the abundance of  $\text{He}^+$  can be derived for each HeI RL as:

$$y^+(\lambda) = \frac{I(\lambda)}{I(\text{H}\beta)} \frac{F_\lambda(n, t)}{f_\lambda(n, t, \tau)} \quad (4.2)$$

where  $F_\lambda(n, t)$  is the theoretical emissivity scaled to  $\text{H}\beta$  and  $f_\lambda$  is the optical depth function. It is generally used the strongest lines, including HeI  $\lambda\lambda$  4471, 5876, 6678 and 7065 Å and then calculating  $y^+$  using a weighted mean, but a precise determination of He abundance requires the use of as many lines as possible (see Peimbert & Luridiana (2002)).

Using PYNEB with the atomic data from Porter et al. (2013) the theoretical emissivities related to  $\text{H}\beta$  can be calculated:

$$\begin{aligned} F_{4471} &= (2.0301 + 1.5 \cdot 10^{-5} \cdot n) \cdot t^{0.1463 - 0.0005 \cdot n} \\ F_{5876} &= (0.745 - 5.1 \cdot 10^{-5} \cdot n) \cdot t^{0.226 - 0.0011 \cdot n} \\ F_{6678} &= (2.612 - 0.000146 \cdot n) \cdot t^{0.2355 - 0.0016 \cdot n} \\ F_{7065} &= (4.329 - 0.0024 \cdot n) \cdot t^{-0.368 - 0.0017 \cdot n} \end{aligned} \quad (4.3)$$

with  $t$  in units of  $10^4$  K and  $n$  in units of  $\text{cm}^{-3}$  and calculated for temperatures between 8000 and 25000 K and densities between 10 and 1000  $\text{cm}^{-3}$ . The precision of the fittings is better than 1% in all case. Normally it is taken the temperature of  $[\text{O III}]$ , as it is the most precise. The optical depth functions can be taken from Olive & Skillman (2004), but these are only important for high-extinction objects and when it is required a very precise measurement of this abundance (e.g. for the search for the primordial helium abundance).

The abundance of  $\text{He}^{2+}$  can be calculated using the HeII 4686 Å line and a high-excitation temperature by means of the recombination coefficients by Storey & Hummer (1995) using the following expression:

$$y^{2+} = \frac{I(4686)}{I(\text{H}\beta)} \cdot 0.0416 \cdot t^{-0.146} \quad (4.4)$$

calculated in the same range as HeI emissivities.

Then, the total He abundance can be derived the addition of the abundances of the two ions:

$$y = y^+ + y^{2+} \quad (4.5)$$

where  $y$  is the relative abundance of helium ( $\text{He}/\text{H}$ ),  $y^+$  the abundance of  $\text{He}^+$ , and  $y^{2+}$  the abundance of  $\text{He}^{2+}$ .

#### 4.2. Oxygen

The chemical abundance of  $O^+$  can be derived with the relative intensity of [O II] 3726, 3729 Å emission lines to  $H\beta$  and the corresponding temperature using the following expression obtained from fittings to PYNEB using the default collision strengths from Pradhan et al.(2006) and Tayal(2007):

$$12 + \log \left( \frac{O^+}{H^+} \right) = \log \left( \frac{I(3726) + I(3729)}{I(H\beta)} \right) + 5.887 + \frac{1.641}{t_l} - 0.543 \cdot \log(t_l) + 0.000114 \cdot n_e \quad (4.6)$$

with a precision better than 0.01dex in the temperature range  $0.7 < t(O^+) < 2.5$  and density of  $100 \text{ cm}^{-3}$ . For a density of  $1000 \text{ cm}^{-3}$  the precision is better than 0.02dex.

Alternatively Kniazev et al.(2003) suggest the use of the 7319,7330 Å doublet in those objects observed with a setup that does not cover the 3727 [O II]line.

$$12 + \log \left( \frac{O^+}{H^+} \right) = \log \left[ \frac{I(7320 + 7330)}{I(H\beta)} \right] + 7.21 + \frac{2.511}{t_l} - 0.422 \cdot \log t_l + 10^{-3.40} n_e (1 - 10^{-3.44} \cdot n_e) \quad (4.7)$$

Regarding  $O^{2+}$ , its chemical abundance was derived using the relative intensity of [O III] 4959, 5007 Å emission lines to  $H\beta$  and the corresponding temperature using the following expression obtained from fittings to PYNEB:

$$12 + \log \left( \frac{O^{2+}}{H^+} \right) = \log \left( \frac{I(4959) + I(5007)}{I(H\beta)} \right) + 6.1868 + \frac{1.2491}{t_h} - 0.5816 \cdot \log(t_h) \quad (4.8)$$

with a precision better than 0.01dex in the temperature range  $0.7 < t(O^{2+}) < 2.5$ . A change in the density from 10 to  $1000 \text{ cm}^{-3}$  implies a decrease of less than 0.01dex in the derived abundance.

The total oxygen abundance can be approximated by

$$\frac{O}{H} = \frac{O^+ + O^{2+}}{H^+} \quad (4.9)$$

given that due to the charge exchange reaction the relative fractions of neutral oxygen and hydrogen are similar:

$$\frac{O^0}{O} = \frac{H^0}{H} \quad (4.10)$$

However, in some high-excitation spectra where the He II 4586 Å is seen it can be considered that part of the O is under the form of  $O^{3+}$ . In that case it can be assumed that:



$$\text{ICF}(O^+ + O^{2+}) = 1 + \frac{y^{2+}}{y^+} \quad (4.11)$$

#### 4.3. Sulfur

The abundances are obtained from the 6717, 6731 Å lines for  $S^+$  and by the 9069, 9532 Å lines for  $S^{2+}$ , though for the latter, also the 6312 Å line can be used using the following expressions:

$$12 + \log\left(\frac{S^+}{H^+}\right) = \log\left(\frac{I(6717) + I(6731)}{I(H\beta)}\right) + 5.463 + \frac{0.941}{t_l} - 0.37 \cdot \log t_l \quad (4.12)$$

and

$$12 + \log\left(\frac{S^{2+}}{H^+}\right) = \log\left[\frac{I(9069) + I(9532)}{I(H\beta)}\right] + 5.983 + \frac{0.661}{t_m} - 0.527 \log(t_m). \quad (4.13)$$

In case that the near-IR [S III] lines cannot be measured but the auroral line at 6312 Å is available with good signal-to-noise, it is possible to derive  $S^{2+}$  abundances from the expression:

$$12 + \log\left(\frac{S^{2+}}{H^+}\right) = \log\left(\frac{I(6312)}{I(H\beta)}\right) + 6.695 + \frac{1.664}{t_m} - 0.513 \cdot \log(t_m) \quad (4.14)$$

These were derived using the same collisional coefficients as used for the derivation of expressions for temperature. The fittings have a precision better than 0.01 dex in the temperature range  $0.7 < t$

The ICF for sulfur takes into account the  $S^{3+}$  abundance which cannot be determined in the optical range. A good approximation is given by Stasińska(1978):

$$\text{ICF}(S^+ + S^{2+}) = \left[1 - \left(\frac{O^{2+}}{O^+ + O^{2+}}\right)^\alpha\right]^{-1/\alpha} \quad (4.15)$$

Although it is customary to write this expression as a function of the  $O^+/(O^+ + O^{2+})$  ionic fraction, we have reformulated it in terms of  $O^{2+}/(O^+ + O^{2+})$  since the errors associated to  $O^{2+}$  are considerably smaller than for  $O^+$ . and for a sample of objects with observed [S IV] line at 10.5  $\mu\text{m}$ , it was derived  $\alpha \approx 3.27$  (Dors et al.(2016)).

#### 4.4. Nitrogen

We can calculate  $N^+$  abundance from the 6548 and 6583 Å lines. The expression to calculate  $N^+/H^+$  abundance using these lines and assuming a low-excitation temperature is:

$$12 + \log\left(\frac{N^+}{H^+}\right) = \log\left(\frac{I(6548) + I(6583)}{I(H\beta)}\right) + 6.291 + \frac{0.90221}{t_l} - 0.5511 \cdot \log(t_l) \quad (4.16)$$

with a precision better than 0.01dex in the temperature range  $0.6 < t < 2.2$ . It decreases less than 0.01dex when the considered density goes from 100 to 1000  $\text{cm}^{-3}$ .

One can calculate quite precisely the total abundance of Nitrogen assuming that:

$$\frac{N^+}{N} = \frac{O^+}{O} \quad (4.17)$$

owing to the similarity of ionization potentials of  $O^+$  and  $N^+$ , what leads to the corresponding ICF:

$$\text{ICF}(N^+) = \frac{O}{O^+} \quad (4.18)$$

The ratio  $N^+/O^+$  can be derived directly from the expression:

$$\log\left(\frac{N^+}{O^+}\right) = \log\left(\frac{I(6583)}{I(3726) + I(3729)}\right) + 0.493 - 0.025 \cdot t_l - \frac{0.687}{t_l} + 0.1621 \cdot \log(t_l) \quad (4.19)$$

#### 4.5. Neon

Ne has [NeIII] prominent emission lines in the blue part of the spectrum and can be a good tracer of metallicity as it is not depleted into dust grains. Since one of the emission lines (3968 Å) usually appears blended with and H $\alpha$  recombination line (H7), the  $\text{Ne}^{2+}$  ionic abundance can be derived using the following expression from the line at 3869 Å and the electron temperature of the high-excitation zone (usually  $t([\text{O III}])$ ):

$$12 + \log\left(\frac{Ne^{2+}}{H^+}\right) = \log\left(\frac{I(3869)}{I(H\beta)}\right) + 6.947 + \frac{1.614}{t_h} - 0.4291 \cdot \log(t_h) \quad (4.20)$$

with a precision better than 2% in the range of temperature from 0.6 to 2.2 in units of  $10^4$  K. The collisional coefficients are from McLaughlin et al.(2000).

The ionization correction factor for neon can be calculated according to the expression given by Pérez-Montero et al.(2007) based on photoionization models:

$$\text{ICF}(Ne^{2+}) = 0.753 + 0.142x + \frac{0.171}{x} \quad (4.21)$$

where  $x = O^{2+}/(O^+ + O^{2+})$ . This expression deviates from the classical approximation  $\text{Ne}/O \approx \text{Ne}^{2+}/O^{2+}$  used to derive total neon abundances.

#### 4.6. Argon

For argon, we use the [ArIII] 7137 Å line. It is possible to measure as well the lines of [ArIV] at 4713 and 4740 Å. Nevertheless, the first of them usually appears blended with another line of HeII at 4711Å that is difficult to correct, so it is better to use the second and brighter to calculate the ionic abundance of Ar<sup>3+</sup>.

$$12 + \log \left( \frac{Ar^{2+}}{H^+} \right) = \log \left( \frac{I(7135)}{I(H\beta)} \right) + 6.100 + \frac{0.86}{t_m} - 0.404 \cdot \log(t_m) \quad (4.22)$$

$$12 + \log \left( \frac{Ar^{3+}}{H^+} \right) = \log \left( \frac{I(4740)}{I(H\beta)} \right) + 6.306 + \frac{1.232}{t_h} - 0.703 \cdot \log(t_h) \quad (4.23)$$

both with a precision better than 2% in the fitting in the same temperature range than in Ne using the collisional coefficients from Galavis et al.(1995) for Ar<sup>2+</sup> and Ramsbottom & Bell(1997) for Ar<sup>3+</sup>.

As in the case of neon, the total abundance of argon can be calculated using the ionization correction factors (ICF(Ar<sup>2+</sup>) and the ICF(Ar<sup>2+</sup>+Ar<sup>3+</sup>)) given by Pérez-Montero et al.(2007). It can be used the first one only when we cannot derive a value for Ar<sup>3+</sup>. The expressions for these ICFs are:

$$ICF(Ar^{2+}) = 0.596 + 0.967(1 - x) + \frac{0.077}{(1 - x)} \quad (4.24)$$

$$ICF(Ar^{2+} + Ar^{3+}) = 0.929 + 0.364(1 - x) + \frac{0.006}{(1 - x)} \quad (4.25)$$

where  $x = O^{2+}/(O^+ + O^{2+})$ .

#### 4.7. Iron

The abundance of Fe is usually derived from the absorption stellar features, but there are some high-excitation [FeIII] lines that can be used to derive Fe<sup>2+</sup> abundances in the ionized gas-phase. For instance, from 4658 Å from PYNEB it is obtained:

$$12 + \log \left( \frac{Fe^{2+}}{H^+} \right) = \log \left( \frac{I(4658)}{I(H\beta)} \right) + 6.288 + \frac{1.408}{t_h} - 0.203 \cdot \log(t_h) \quad (4.26)$$

using the collisional coefficients of Fe<sup>2+</sup> from Zhang(1996) in the range  $t = 0.8 - 2.5$ . The ICF to derive the total Fe abundance was proposed by Rodríguez & Rubin(2004):

$$ICF(Fe^{2+}) = \left( \frac{O^+}{O^{2+}} \right)^{0.09} \left[ 1 + \frac{O^{2+}}{O^+} \right] \quad (4.27)$$

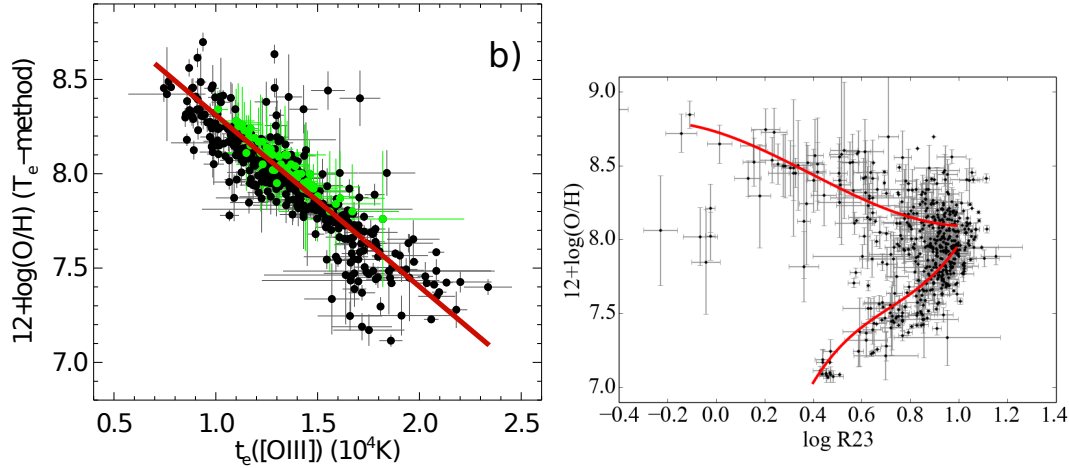


FIGURE 7. Left panel: Empirical relation between electron temperature and total oxygen abundance (Amorín et al.(2015)). Right panel, relation between oxygen abundance and the R23 parameter from the sample of objects in Pérez-Montero & Contini(2009) and non-linear fittings for the lower and upper branches assuming the average excitation in each range.

## 5. Strong-line methods calibrated using the DM

In absence on any of the auroral lines it is not possible to obtain the electron temperature, and hence to derive the thermal structure and the ionic and total abundances of the elements whose lines can be measured in the optical spectrum. However, some of the other nebular CELs can be measured and be used as indicators of the chemical content of the gas.

As quoted above, many of the calibrations of these so-called strong-line methods have been made in the literature attending to different criteria or calibration sample so it is difficult to assess if they are compatible between them. The most important rule to follow is try to be consistent if we want to make a comparative analysis. In this section I describe different strong-line methods calibrated with large samples of objects with a previous determination of the electron temperature so they are in principle compatible with the direct method. For the sake of consistency, it is only here cited those calibrations calculated using the same methodology as described in the above sections and using a very similar sample of objects, selected only with criterion of having at least one measured electron temperature, be ionized by massive star formation, and with no restriction on the resulting chemical abundances. However, it is worth to mention the existence of other calibrations based on the direct method such as Pilyugin et al.(2010), Pilyugin & Grebel(2016) or Marino et al.(2013), among others.

### 5.1. Calibrations of the electron temperature

Sometimes it is possible to derive an electron temperature and its corresponding ionic abundance. Nevertheless, the total abundance cannot be calculated because the lines corresponding to other excitation lines cannot be measured. This is the case of O/H when the  $[\text{O II}]$  3727 Å lines are out of the spectral range or their corresponding auroral lines at 7319 and 7330 Å are too faint.

In this case the total oxygen abundance can be estimated directly from the  $[\text{O III}]$  electron temperature as proposed by Amorín et al.(2015) and that can be seen in left panel of Fig.7:

$$12 + \log(O/H) = 9.22(\pm 0.03) - 0.89(\pm 0.02) \cdot t([O\text{ III}]) \quad (5.1)$$

with a dispersion of 0.15 dex. This expression can also be used to derive the temperature from a strong-line derivation of O/H. The electron temperature is useful for example to quantify the extinction from the Balmer decrement.

### 5.2. Parameters based on $[O\text{ II}]$ and $[O\text{ III}]$ lines

The most widely used parameter based on oxygen lines that can be related to metallicity is R23 given by Pagel et al.(1979):

$$R23 = \frac{I(3727) + I(4959, 5007)}{I(H\beta)} \quad (5.2)$$

However, there are some known limitations to give a calibration of this parameter with O/H. The main limitation is that the relation is double-valued: R23 grows with O/H for low-Z and it decreases for high-Z, as the main source of cooling when the temperature is lower are hydrogen recombination lines. In the so-called turnover region (around  $12 + \log(O/H) \approx 8.0 - 8.3$ , as can be seen in right panel of Fig. 7) the dispersion is very high and it is very difficult to provide an accurate determination.

For this tutorial and for the sake of consistency I provide fittings to the sample of objects with a direct determination of O/H in Pérez-Montero & Contini(2009), following the same functional expressions given by Kobulnicky et al.(1999) based on R23 and on the excitation as a function of the ratio of  $[O\text{ II}]$  and  $[O\text{ III}]$ . The fittings for both branches at an average excitation in each branch are shown in Fig. 7.

In the upper branch ( $12 + \log(O/H) > 8.25$ ):

$$12 + \log(O/H) = 8.656 - 0.411 \cdot x - 0.586 \cdot x^2 + 0.469 \cdot x^3 - \\ - y \cdot (-0.224 + 0.309 \cdot x + 0.741 \cdot x^2 + 0.722 \cdot x^3) \quad (5.3)$$

where  $x = \log(R23)$  and  $y = \log([O\text{ II}]3727/[O\text{ III}]4959+5007)$ . The dispersion of this fitting, taken as the standard deviation of the residuals to the abundances from the direct method is 0.17 dex.

For the lower branch ( $12 + \log(O/H) < 8.0$ ):

$$12 + \log(O/H) = 7.247 - 1.196 \cdot x + 4.078 \cdot x^2 - 2.194 \cdot x^3 - \\ - y \cdot (1.076 - 3.735 \cdot x + 5.671 \cdot x^2 - 2.947 \cdot x^3) \quad (5.4)$$

with a dispersion of 0.14 dex.

In cases where the  $[O\text{ III}]$  are not observed owing the studied spectral range, Pérez-Montero et al.(2007) propose to use the empirical relation with  $[Ne\text{ III}]$  at 3968 Å (=  $[O\text{ III}] 5007 / 15.37$ ) and using also a hydrogen recombination line at a blue wavelength, such as  $H\gamma$  or  $H\delta$ .

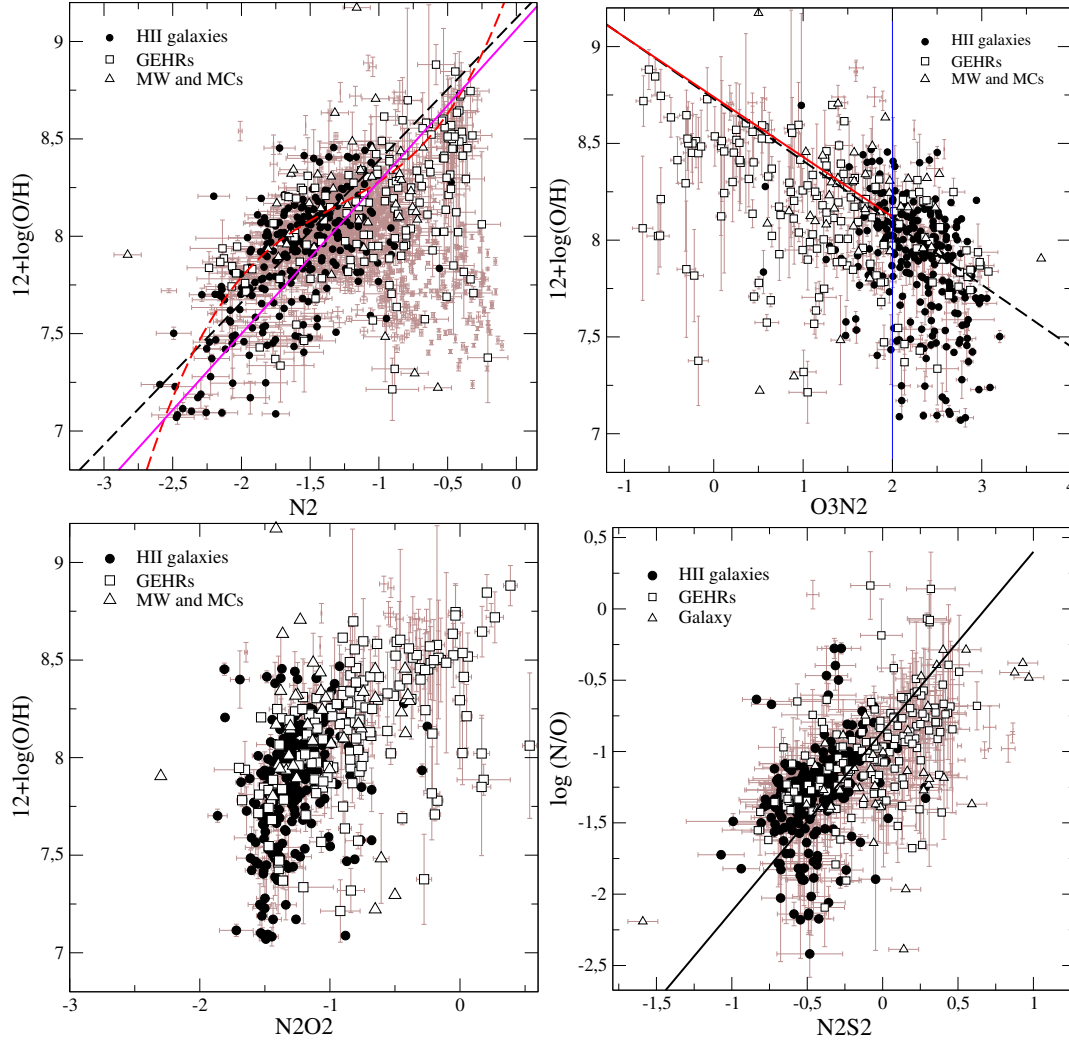


FIGURE 8. Relations between strong-line parameters based on  $[\text{N II}]$  emission-lines and ionic ratios from Pérez-Montero & Contini(2009). From left to right and from up to down: N2 with O/H, O3N2 with O/H, N2O2 with N/O, and N2S2 with N/O.

### 5.3. Parameters based on $[\text{N II}]$ lines

The most simple strong line ratio used to derive O/H using  $[\text{N II}]$  lines is the N2 parameter, defined by Storch-Bergmann et al.(1994):

$$N2 = \log \left( \frac{I(6583)}{I(H\alpha)} \right) \quad (5.5)$$

Notice that, contrary to R23, the log is in the definition of the parameter. This parameter has at the advantage to be totally independent on reddening correction or flux calibration uncertainties. The linear fitting proposed by Pérez-Montero & Contini(2009) gives:

$$12 + \log(O/H) = 9.07 + 0.79 \cdot N2 \quad (5.6)$$

valid for all the range of metallicity with a dispersion of 0.34 dex. This relation can be seen in Fig. 8. This is usually used to decide to the branch of the R23 parameter, but the dispersion is very high owing to a large dependence on ionization parameter and also to the dispersion in the O/H-N/O relation.

The dependence on  $\log U$  can be reduced through the definition of the O3N2 parameter (Alloin et al.(1979)):

$$O3N2 = \log \left( \frac{I(5007)}{I(H\beta)} \cdot \frac{I(H\alpha)}{I(6583)} \right) \quad (5.7)$$

The linear fitting proposed by Pérez-Montero & Contini(2009) leads to:

$$12 + \log(O/H) = 8.74 - 0.31 \cdot O3N2 \quad (5.8)$$

with a dispersion of 0.32 dex, but for  $O3N2 > 2.0$  as the O3N2 parameter is constant for lower metallicities, as can be seen in Fig. 8.

Among other strong emission line ratios the parameter N2O2:

$$N2O2 = \log \left( \frac{I(6583)}{I(3727)} \right) \quad (5.9)$$

can be used to derive N/O, as can be seen in Fig. 8. The linear fitting proposed by Pérez-Montero & Contini(2009) gives:

$$\log(N/O) = 0.93 \cdot N2O2 - 0.20 \quad (5.10)$$

with a dispersion of 0.24 dex for all N/O values. A similar parameter for a lower wavelength baseline is the N2S2 parameter:

$$N2S2 = \log \left( \frac{I(6583)}{I(6717, 6731)} \right) \quad (5.11)$$

whose linear fitting gives:

$$\log(N/O) = 1.26 \cdot N2S2 - 0.86 \quad (5.12)$$

with a dispersion of 0.31 dex according to Pérez-Montero & Contini(2009).

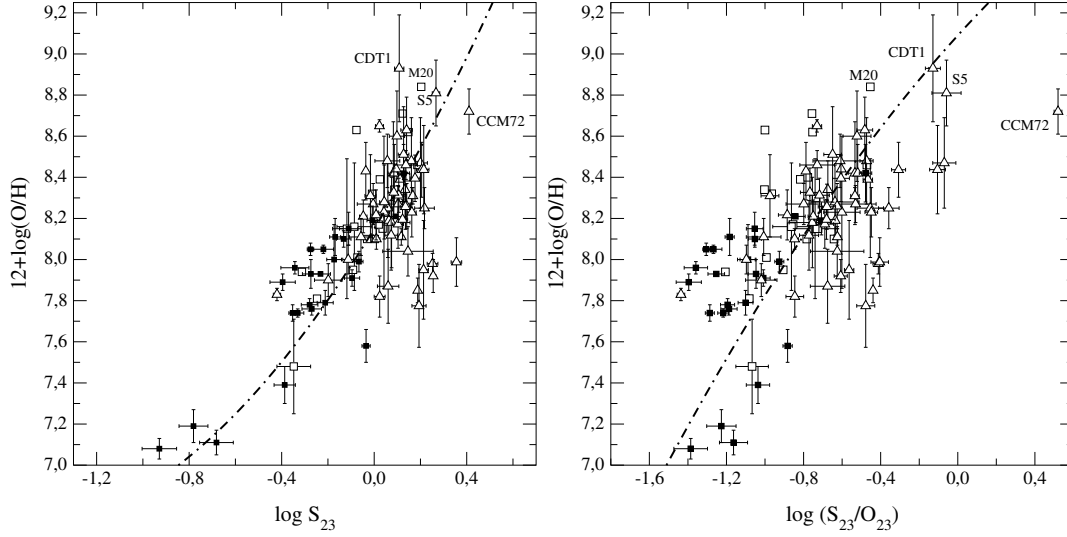


FIGURE 9. Relations and calibrations between the total oxygen abundance and the S23 parameter (left) and S23/R23 parameter (right) from Pérez-Montero & Díaz(2005).

#### 5.4. Parameters based on $[S\text{II}]$ and $[S\text{III}]$ lines

Strong-line methods based on sulfur emission lines provide accurate oxygen abundances when the red and near-IR spectral optical range is observed and measured. This is based on the fact that both O and S are primary elements and hence the S/O ratio is expected to not vary. Following an analogous definition as for oxygen lines, Vilchez & Esteban(1996) defined the S23 parameter based on  $[S\text{II}]$  and  $[S\text{III}]$  lines as:

$$S23 = \frac{I(6717, 6731) + I(9099, 9532)}{I(H\beta)} \quad (5.13)$$

The polynomial fitting proposed by Pérez-Montero & Díaz(2005) to derive total oxygen abundance is:

$$12 + \log(O/H) = 8.15 + 0.85 \cdot x + 0.58 \cdot x^2 \quad (5.14)$$

where  $x = \log(S23)$ . This can be used up to solar metallicity (i.e.  $12 + \log(O/H) = 8.69$ ) with a dispersion of 0.20 dex as the standard deviation of the residuals to the O/H derived from the direct method. This relation can be seen in left panel of Fig. 9. Similarly Pérez-Montero et al.(2006) propose a fitting to derive total sulfur abundances:

$$12 + \log(S/H) = 6.622 + 1.860 \cdot x + 0.382 \cdot x^2 \quad (5.15)$$

with a dispersion of 0.185 dex in the range of  $-1.0 \leq \log(S23) \leq 0.5$ .

For high metallicities Pérez-Montero & Díaz(2005) propose a polynomial fitting to a combination of both S12 and R23, as can be seen in right panel of Fig. 9. This fitting gives:



$$12 + \log(O/H) = 9.09 + 1.03 \cdot x - 0.22 \cdot x^2 \quad (5.16)$$

where  $x = \log(S23/R23)$  and the fitting to the objects has a dispersion of 0.27 dex.

## 6. Summary

In this tutorial it has been reviewed the procedure to analyze the optical emission-line spectrum from a gaseous nebula ionized by massive star formation. Both recombination lines emitted from H and He, and collisionally excited emission lines from metallic ions can be used to derive the physical properties and the ionic and total abundances using the so-called direct method. To do so, it has been provided expressions derived from the software PYNEB (Luridiana et al.(2012)) under typical conditions observed in H II regions and using the most updated sets of atomic coefficients.

The direct method relies on the determination of the electronic temperature using the emission-line ratios between strong nebular lines and faint auroral emission lines. It is also assumed that the complete ionization structure is comprised in the observed spectrum. In this situation one can calculate the thermal and density radial structure of the distribution of ionized gas, measuring as many temperatures as possible and solving their dependence on density. Alternatively, one can assume relations between zone temperatures from empirical or model-based relations. Then the ionic abundances for the corresponding emission lines observed in the spectrum can be derived. Finally, the total chemical abundances are calculated by means of ionization correction factors that are used to derive the abundances of the ions not seen in the observed spectrum.

In case that no auroral lines are observed in the optical spectrum, one can resort to strong-line methods based on the measurement of the nebular lines. These methods lead formally to determinations of the abundances much less accurate than the direct method due to additional dependences of the involved lines on other functional parameters (e.g. Pérez-Montero & Díaz(2005)). However, the most important is that any comparison between abundances derived from the direct method and from strong-line calibrations is done consistently. This can happen for datasets where the auroral lines are not observed in all points. In this case strong-line methods calibrated empirically or using models consistent with the direct method are convenient.

## Acknowledgements

This tutorial has been done thanks to the financial supports from MINECO Project AYA2013-47742-C4-1-P and AYA2016-79724-C4-4-P of the Spanish Plan for Astronomy and astrophysics. I also thank Rubén García-Benito for his kind revision of the manuscript and to a anonymous referee whose comments have helped to improve the final manuscript.

## REFERENCES

- Aggarwal, K. M. & Keenan, F. P. 1999, *ApJS*, 123, 311  
 Alloin, D., Collin-Souffrin, S., Joly, M., & Vigroux, L. 1979, *A&A*, 78, 200  
 Amorín, R., Pérez-Montero, E., Contini, T., et al. 2015, *A&A*, 578, A105  
 Baldwin, J. A., Phillips, M. M., & Terlevich, R. 1981, *PASP*, 93, 5  
 Calzetti, D., Armus, L., Bohlin, R. C., et al. 2000, *ApJ*, 533, 682  
 Cardelli, J. A., Clayton, G. C., & Mathis, J. S. 1989, *ApJ*, 345, 245

- Castellanos, M., Díaz, Á. I., & Tenorio-Tagle, G. 2002, *ApJL*, 565, L79
- Cid Fernandes, R., Mateus, A., Sodré, L., Stasińska, G., & Gomes, J. M. 2005, *MNRAS*, 358, 363
- Dors, O. L., Pérez-Montero, E., Hägele, G. F., Cardaci, M. V., & Krabbe, A. C. 2016, *MNRAS*, 456, 4407
- Dors, Jr., O. L., Krabbe, A., Hägele, G. F., & Pérez-Montero, E. 2011, *MNRAS*, 415, 3616
- Fernández-Martín, A., Pérez-Montero, E., Vílchez, J. M., & Mampaso, A. 2017, *A&A*, 597, A84
- Galavis, M. E., Mendoza, C., & Zeppen, C. J. 1995, *A&AS*, 111, 347
- Garnett, D. R. 1992, *AJ*, 103, 1330
- Gonzalez-Delgado, R. M., Perez, E., Tenorio-Tagle, G., et al. 1994, *ApJ*, 437, 239
- , K. D., Clayton, G. C., Misselt, K. A., Landolt, A. U., & Wolff, M. J. 2003, *ApJ*, 594, 279
- Hägele, G. F., Pérez-Montero, E., Díaz, Á. I., Terlevich, E., & Terlevich, R. 2006, *MNRAS*, 372, 293
- Hudson, C. E., Ramsbottom, C. A., & Scott, M. P. 2012, *ApJ*, 750, 65
- Kewley, L. J. & Ellison, S. L. 2008, *ApJ*, 681, 1183
- Kewley, L. J., Groves, B., Kauffmann, G., & Heckman, T. 2006, *MNRAS*, 372, 961
- Kniazev, A. Y., Grebel, E. K., Hao, L., et al. 2003, *ApJL*, 593, L73
- Kobulnicky, H. A., Kennicutt, Jr., R. C., & Pizagno, J. L. 1999, *ApJ*, 514, 544
- Liu, X.-W., Luo, S.-G., Barlow, M. J., Danziger, I. J., & Storey, P. J. 2001, *MNRAS*, 327, 141
- López-Sánchez, Á. R., Westmeier, T., Esteban, C., & Koribalski, B. S. 2015, *MNRAS*, 450, 3381
- Luridiana, V., Morisset, C., & Shaw, R. A. 2012, in *IAU Symposium*, Vol. 283, *IAU Symposium*, 422–423
- Luridiana, V., Peimbert, M., & Leitherer, C. 1999, *ApJ*, 527, 110
- Marino, R. A., Rosales-Ortega, F. F., Sánchez, S. F., et al. 2013, *A&A*, 559, A114
- McLaughlin, B. M., Gorczyca, T. W., Keenan, F. P., & Bell, K. L. 2000, *JPhB*, 33, 597
- Olive, K. A. & Skillman, E. D. 2004, *ApJ*, 617, 29
- Osterbrock D. E., Ferland G. J., 2006, *agna.book*,
- Pagel, B. E. J., Edmunds, M. G., Blackwell, D. E., Chun, M. S., & Smith, G. 1979, *MNRAS*, 189, 95
- Pagel, B. E. J., Simonson, E. A., Terlevich, R. J., & Edmunds, M. G. 1992, *MNRAS*, 255, 325
- Peimbert, A. 2003, *ApJ*, 584, 735
- Peimbert, A., Peimbert, M., & Luridiana, V. 2002, *ApJ*, 565, 668
- Peimbert, M., Luridiana, V., & Peimbert, A. 2007, *ApJ*, 666, 636
- Pérez-Montero, E. 2003, PhD thesis, PhD Thesis, 2003
- Pérez-Montero, E. 2014, *MNRAS*, 441, 2663
- Pérez-Montero, E. & Contini, T. 2009, *MNRAS*, 398, 949
- Pérez-Montero, E. & Díaz, A. I. 2003, *MNRAS*, 346, 105
- Pérez-Montero, E. & Díaz, A. I. 2005, *MNRAS*, 361, 1063
- Pérez-Montero, E. & Díaz, Á. I. 2007, *MNRAS*, 377, 1195
- Pérez-Montero, E., Díaz, A. I., Vílchez, J. M., & Kehrig, C. 2006, *A&A*, 449, 193
- Pérez-Montero, E., García-Benito, R., Díaz, A. I., Pérez, E., & Kehrig, C. 2009, *A&A*, 497, 53
- Pérez-Montero, E., Hägele, G. F., Contini, T., & Díaz, Á. I. 2007, *MNRAS*, 381, 125
- Pilyugin, L. S. & Grebel, E. K. 2016, *MNRAS*, 457, 3678
- Pilyugin, L. S., Vílchez, J. M., & Thuan, T. X. 2010, *ApJ*, 720, 1738
- Porter, R. L., Ferland, G. J., Storey, P. J., & Detisch, M. J. 2013, *MNRAS*, 433, L89
- Pradhan, A. K., Montenegro, M., Nahar, S. N., & Eissner, W. 2006, *MNRAS*, 366, L6
- Ramsbottom, C. A. & Bell, K. L. 1997, *Atomic Data and Nuclear Data Tables*, 66, 65
- Rodríguez, M., & Rubin, R. H. 2004, *Recycling Intergalactic and Interstellar Matter*, 217, 188
- Sánchez, S. F., Pérez, E., Rosales-Ortega, F. F., et al. 2015, *A&A*, 574, A47
- Stasińska, G. 1978, *A&A*, 66, 257
- Stasińska, G. 1990, *A&AS*, 83, 501
- Storchi-Bergmann, T., Calzetti, D., & Kinney, A. L. 1994, *ApJ*, 429, 572
- Storey, P. J. & Hummer, D. G. 1995, *MNRAS*, 272, 41
- Tayal, S. S. 2007, *ApJS*, 171, 331

- Tayal, S. S. 2011, ApJS, 195, 12  
Tayal, S. S. & Zatsarinny, O. 2010, ApJS, 188, 32  
Vilchez, J. M. & Esteban, C. 1996, MNRAS, 280, 720  
Zhang, H. 1996, A&AS, 119, 205